Geo-Mar Lett (2008) 28:53–64
DOI 10.1007/s00367-007-0089-8

ORIGINAL

# The role of basement inheritance faults in the recent fracture system of the inner shelf around Alboran Island, Western Mediterranean

**A. Maestro-González · P. Bárcenas · J. T. Vázquez · V. Díaz-del-Río**

Received: 7 April 2006 / Accepted: 15 June 2007 / Published online: 25 July 2007


**Abstract** Fractures associated with volcanic rock outcrops on the inner shelf of Alboran Island, Western Mediterranean, were mapped on the basis of a side-scan sonar mosaic. Absolute maximum fracture orientation frequency is NW–SE to NNW–SSE, with several sub-maxima oriented NNE–SSW, NE–SW and ENE–WSW. The origin of the main fracture systems in Neogene and Quaternary rocks of the Alboran Basin (south Spain) appears to be controlled by older structures, namely NE–SW and WNW–ESE to NW–SE faults which cross-cut the basement. These faults, pre-Tortonian in origin, have been reactivated since the early Neogene in the form of strike-slip and extensional movements linked to the recent stress field in this area. Fracture analysis of volcanic outcrops on the inner continental shelf of Alboran Island suggests that the shelf has been deformed into a narrow shear zone limited by two NE–SW-trending, sub-parallel high-angle faults, the main orientation and density of which have been influenced by previous WNW–ESE to NW–SE basement fractures.

A. Maestro-González (✉)
Servicio de Geología Marina,
Instituto Geológico y Minero de España,
Rios Rosas 23,
28003 Madrid, Spain
e-mail: a.maestro@igme.es

P. Bárcenas · V. Díaz-del-Río
Instituto Español de Oceanografía,
Apartado 285,
29640 Fuengirola, Málaga, Spain

J. T. Vázquez
Departamento de Geología, Facultad de Ciencias del Mar,
Universidad de Cádiz,
Campus Río San Pedro,
11510 Puerto Real, Cádiz, Spain

## Introduction

Reactivation of ancient faults, a common mechanism of deformation in the brittle crust, depends mainly on the action of a new, different stress field and the direction, dip and strength of the faults. In strongly deformed areas, fault reactivation may lead to basin inversion or development of pull-apart or extensional basins (De Graciansky et al. 1989; Williams et al. 1989). In weakly deformed intra-cratonic areas, fault reactivation can lead to the fracturing of cover units overlying the basement. Surface fracture patterns resulting from reactivation of deep-seated faults in the basement depend on (1) the kinematic nature of the fault, i.e. strike-slip, normal or reverse. In the case of strike-slip faults R, R′ and T fractures are formed in the surface cover (Riedel 1929; Tchalenko 1970; Naylor et al. 1986; Mandl 1988). Normal or reverse basement faults tend to produce surface faults parallel to the underlying basement faults (Mandl 1988; Withjack et al. 1990). Surface fracture patterns also depend on (2) the rheological properties of the overlying sequence (unilayer or multilayer; Horsfield 1977; Mandl 1988) which mainly control the width of the deformed zone of the overlying basement fault cover.

In the Western Mediterranean, the Alboran Ridge, the most distinctive Alboran Basin feature, cuts the basin obliquely in a NE–SW direction. This structure is an anticlinorium trending N065E, bounded by two major left-lateral strike-slip fault systems, one in the north and one in the south. The water depth to the ridge becomes shallower towards the northeast in the central Alboran Sea, where the ridge crest breaks the water surface to form the Alboran Island (Fig. 1a). Due to the scarcity of sediments, the relative homogeneity of rock type and the simplicity of bedrock structure, the volcanic rock outcrops around

Alboran Island are ideally suited for the study of fractures and their relationship with geological structures (Fig. 1b).

The objectives of this study are (1) to define the fracture pattern of volcanic rock forming the inner continental shelf of the Alboran Island on the basis of side-scan sonar images, and (2) to establish the origin and distribution of the fracture patterns within the older and more recent tectonic framework.

## Geological setting

The Recent/Neogene evolution of the Alboran Basin is related to the continental collision generated by the northward movement of the African plate relative to Iberia, which resulted in westward thrusting and subsequent extension of the Alboran Block, and the creation of oceanic crust in the south-western Algero–Balearic basin plain (Rehault et al. 1985; Dewey et al. 1989; Mauffret et al. 1992).

The Alboran Basin region has been under continuous N–S to NW–SE compression since the Tortonian at least, and probably much earlier (Ott d'Estevou and Montenat 1985; Philip 1987; Sanz de Galdeano 1990; Srivastava et al. 1990; Roest and Srivastava 1991). Since that time, the actual axis of maximum compression seems to have varied, from about NW–SE in the Tortonian to N–S from the late Tortonian to early Pliocene, reverting to about NW–SE in the Pliocene (De Larouzière et al. 1988; Sanz de Galdeano 1990) and with a return also to NW–SE in more recent times (De Mets et al. 1990).

The predominant trend of the most important faults in the Alboran Basin is east–northeast to northeast (Campos et al. 1992; Woodside and Maldonado 1992; Fig. 1a). Other fault systems are oriented north–northwest and east–southeast (Maldonado et al. 1992). Both margins of one of the most relevant structures in the central Alboran Basin, the Alboran Ridge, are affected by faults trending in the same predominantly north-eastern direction. This system is probable the offshore extension of the Jebha Fault, which separates two major structural domains of the Rif Cordillera: the eastern External Rif and the Internal Rifian zones (Leblanc 1990). Land studies have demonstrated that all these faults have a major left-lateral strike-slip component (De Larouzière et al. 1988). The structure of this faulting offshore along the northern margin of the Alboran Ridge may be reverse or strike-slip, with a compressive component (Bourgois et al. 1992; Campos et al. 1992). The ridge itself is truncated along its flanks by several major faults (Fig. 1a). The northern flank is bounded by a major fault escarpment extending roughly WNW–ESE (Dillon et al. 1980; Mauffret et al. 1987). This fault is inferred to have a substantial reverse component, the origin of the progressively higher elevation of the Alboran Ridge towards its northern end culminating in the Alboran Island (Woodside and Maldonado 1992). Moreover, Woodside and Maldonado (1992) describe the presence of at least one fault which compartmentalizes the central sector of the ridge, with a WNW–ESE direction. Some active reverse or right-lateral strike-slip faults with a compressive component have been suggested, the northern side having been elevated higher.

In the northern sector of the Alboran Ridge, Alboran Island is located in the centre of a NE-SW-oriented shoal area (continental shelf), which is ellipsoidal and elongate in shape. The shelf is widest on the north-eastern side, tapering from 17 to 2 km in width; the shelf break is at an average depth of 110 m. Its slope is steeper towards the southeast, with a mean gradient of 13°. In this area, two major canyons with associated turbidite systems, and tectonic and gravitational morphology have been identified (Bárcenas et al. 2000). North-western slope gradients are gentle, about 5°. The asymmetry of the south-eastern slope gradient relative to that of the north-western slope is due to recent tectonic activity which has significantly affected the morphology and sedimentary processes on the south-eastern slope (Bárcenas et al. 2000).

Alboran Island and its shelf consist primarily of pyroclastic volcanic material such as ash flow tuffs and blocks as well as ash flow deposits, overlain by Neogene–Quaternary sedimentary units. The volcanic rock deposits are very similar to those outcropping onshore in the strato-volcanic complex of Cabo de Gata (southeast Spain) and Ras Tarf (northern Morocco), which form a NE–SW-oriented belt of calc-alkaline volcanic rocks. The pyroclastic bed direction is ENE–WSW, and the dip is towards the north (Hernández-Pacheco and Ibarrola 1970); the age of these rocks has been estimated to be between 9.26±0.02 and 9.37±0.01 Ma (Duggen et al. 2004).

## Methods

This study is based on a network of 39 side-scan sonar (EG&G, 500 kHz) tracks obtained in September 1994 during the Alboran 9409 cruise on board the B/O F.P. Navarro (Instituto Español de Oceanografía, Fuengirola, Spain; Fig. 2a). These tracks around Alboran Island were spaced about 200 m apart, comprise a total length of more than 120 km up to a depth of 60 m, and were aligned SW–NE and WNW–ESE to cover the inner continental shelf of the island.

The large number of fractures identified in this survey (Fig. 2b) was classified by means of an automatic

exploration program. This program reads vectorial files (DXF in our case) and explores, systematically, first along the *x*-axis and then along the *y*-axis, generating a file which provides, among other things, the length and orientation of each line. Other conventional statistical programs were run on these data for fracture analysis.

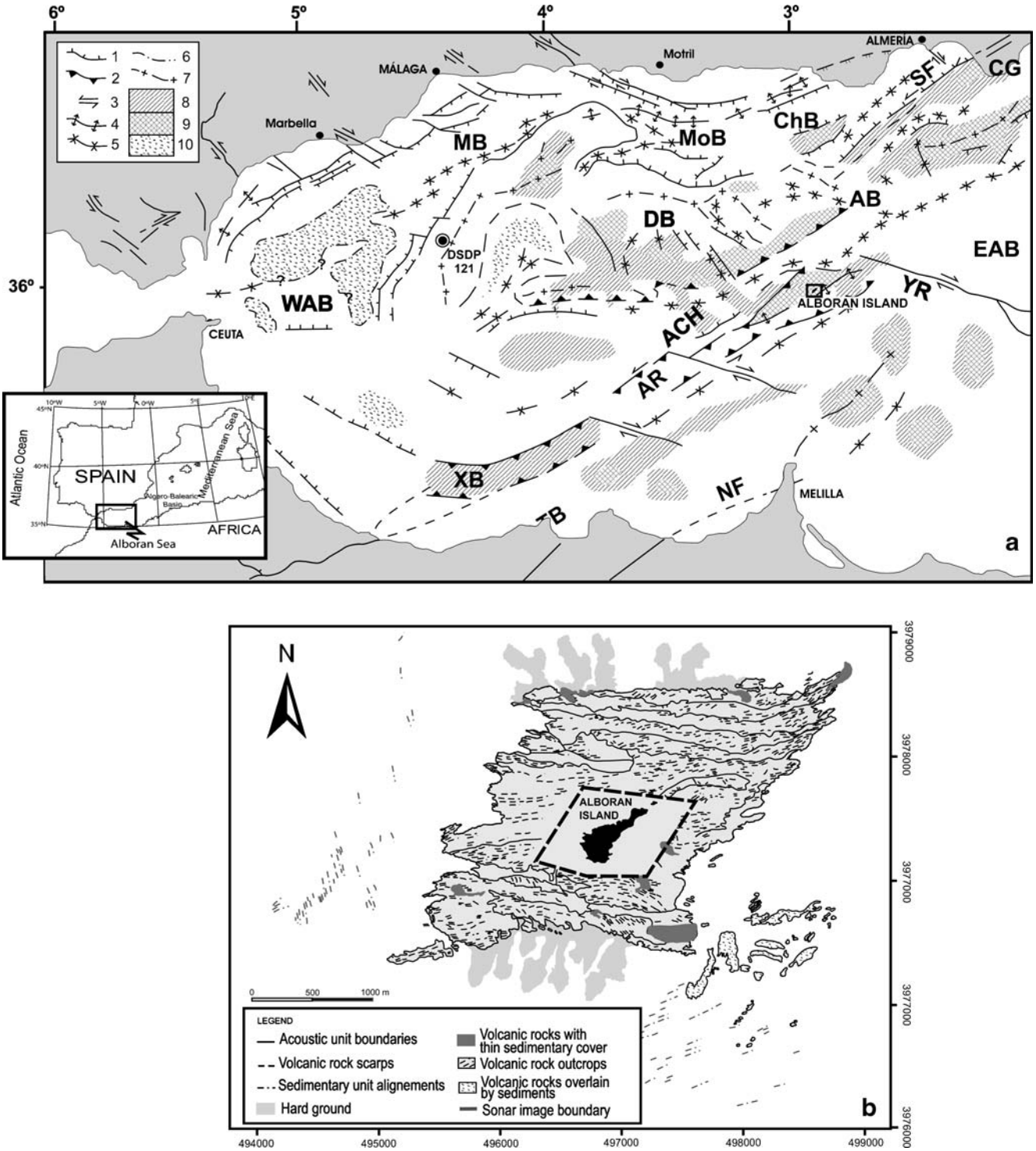


**Fig. 1** **a** Structural scheme of the Alboran Sea. *1* Normal faults, *2* reverse faults, *3* strike–slip components, *4* anticlines, *5* axis of depocentres with maximum sediment thicknesses, *6* boundary of diapiric bodies, *7* basement highs, *8* basement (presumed volcanic), *9* volcanic basement outcropping or sub-outcropping, *10* diapirs, *ACH* Alboran Channel, *AR* Alboran Ridge, *DB* Djibouti Bank, *EAB* Eastern Alboran Basin, *WAB* Western Alboran Basin, *YR* Yusuf Ridge, *JB* Jebha Fault, *NF* Nekor Fault, *XB* Xauen Bank, *TB* Tofiño Bank, *RT* Ras Tarf, *MB* Malaga Basin, *MoB* Motril Basin, *ChB* Chella Bank, *AB* Almeria Basin, *SF* Serrata Fault, *CB* Cabo de Gata (modified from Comas et al. 1992). **b** Detailed geological map of the study area

Fracture density maps displaying fracture distribution are drawn from calculations of the length of lines contained within cells, in a network, divided by cell area. From the data file bearing the coordinates of the beginning and end of each fracture, the number of fractures beginning or ending within each cell is calculated. To archive this, an automatic computation program able to determine the length of fractures, or the length of segments of fractures included within each cell, was used (program Lindens; Casas et al. 2000).

The compilation of fracture density maps begins with the determination of the most appropriate cell size. Critical grid

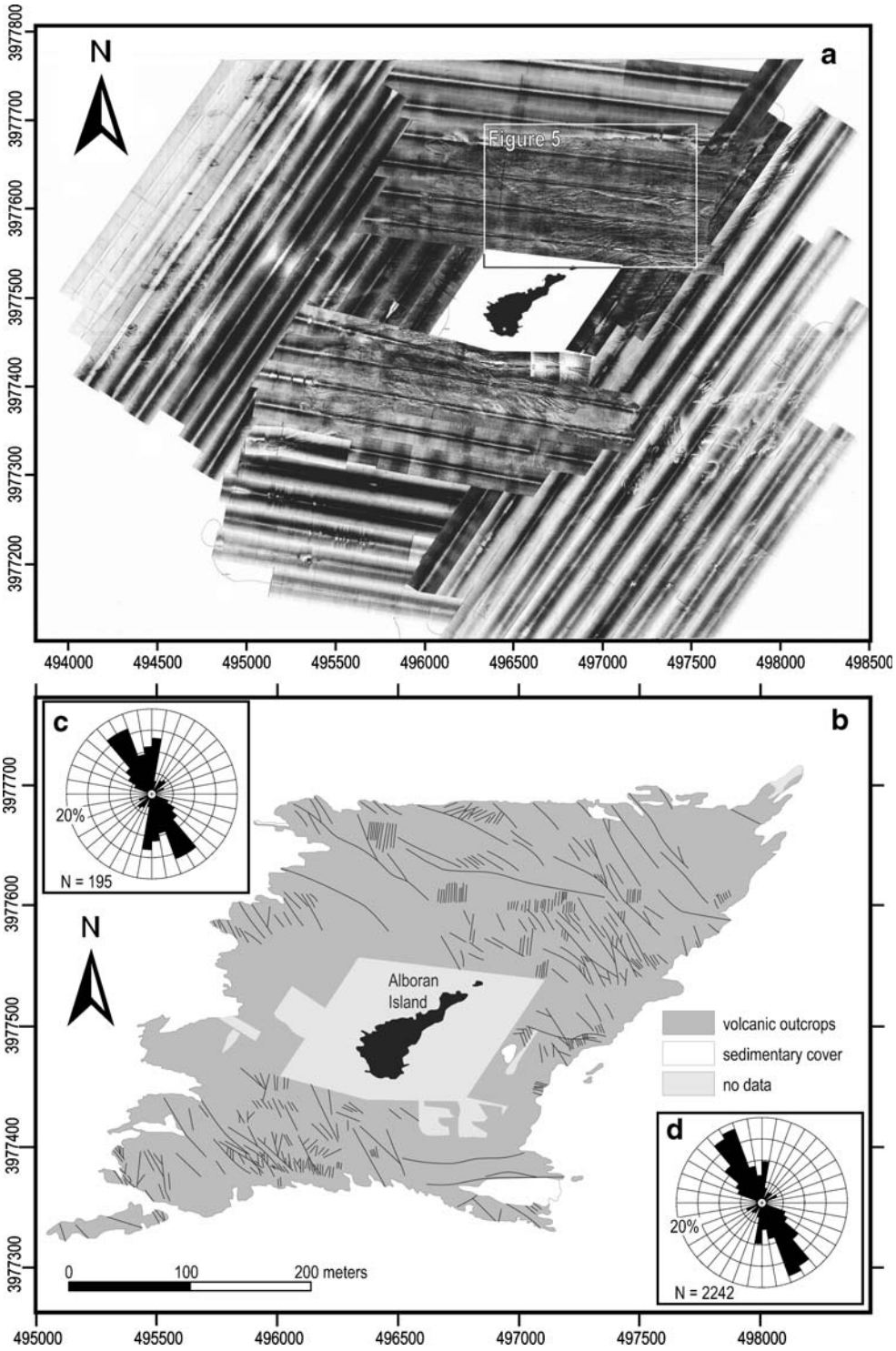


**Fig. 2** **a** Side-scan sonar mosaic. **b** Fracture sketch identified for the Alboran Island inner shelf. **c** Rose diagram of fracture orientation in the study area. **d** Rose diagram of fracture orientation, having weighted fracture trace length

size is conditioned by the average size of fractures and the distance between them. To determine these distances, the Delaunay triangulation method (Preparata and Shamos 1985) was applied. Each fracture is represented by its mid-point. The vertices of Delaunay triangles are constituted by these mid-points. The distance from each fracture (point) to its two nearest neighbours is then calculated. The average distance between three fractures is taken to be the arithmetic mean of the three sides of the triangle, and plotted at the centre of each triangle (Fig. 3a), calculated by

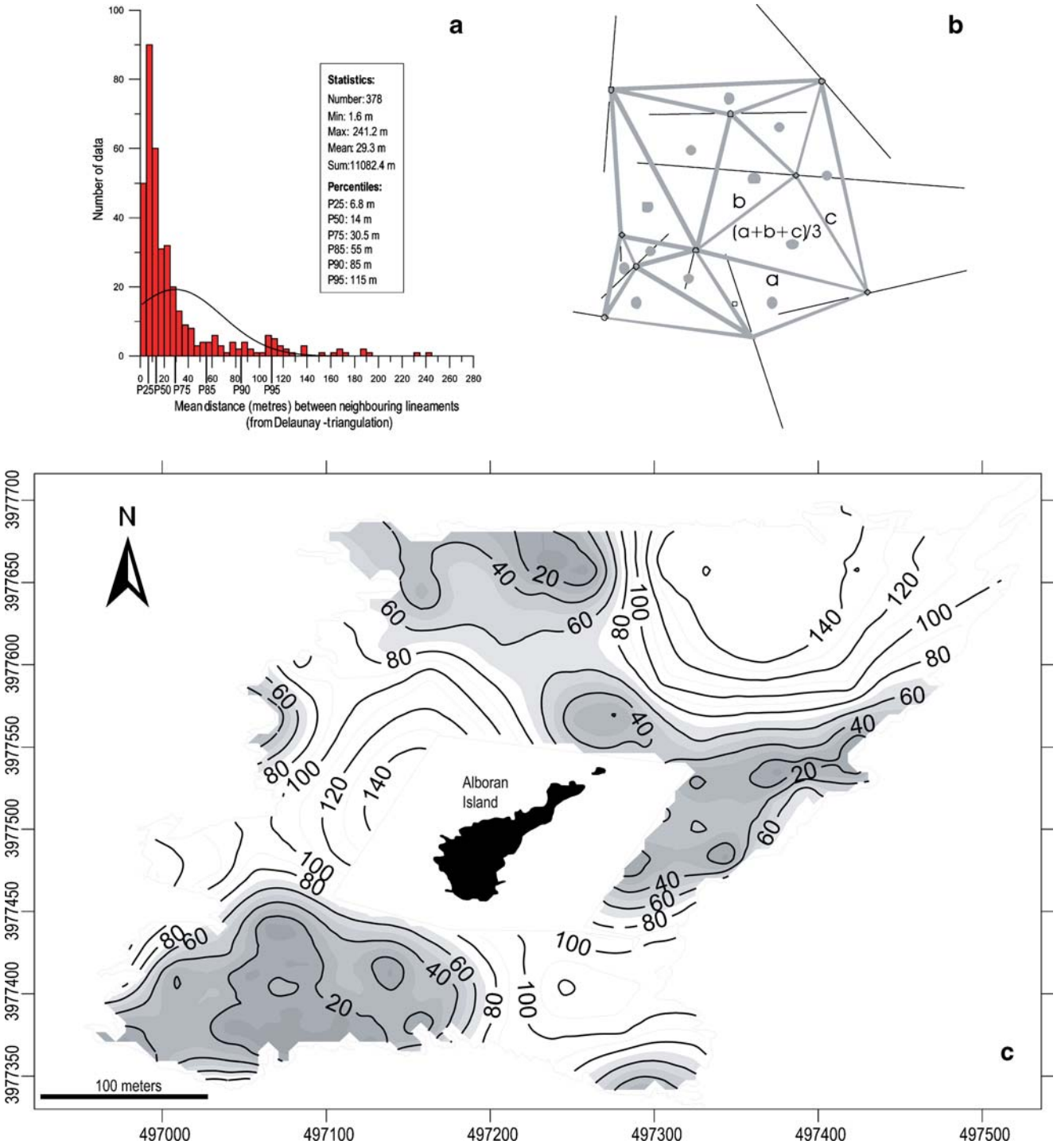


**Fig. 3** **a** Contour map of average distances between fractures in volcanic rock outcrops of the Alboran Island inner shelf. Isoline values represent distance in meters. *Gray areas* indicate an average distance of less than 60 m between fractures. **b** Delaunay triangulation method used to calculate the average distance between fractures. **c** Histogram of the distances calculated

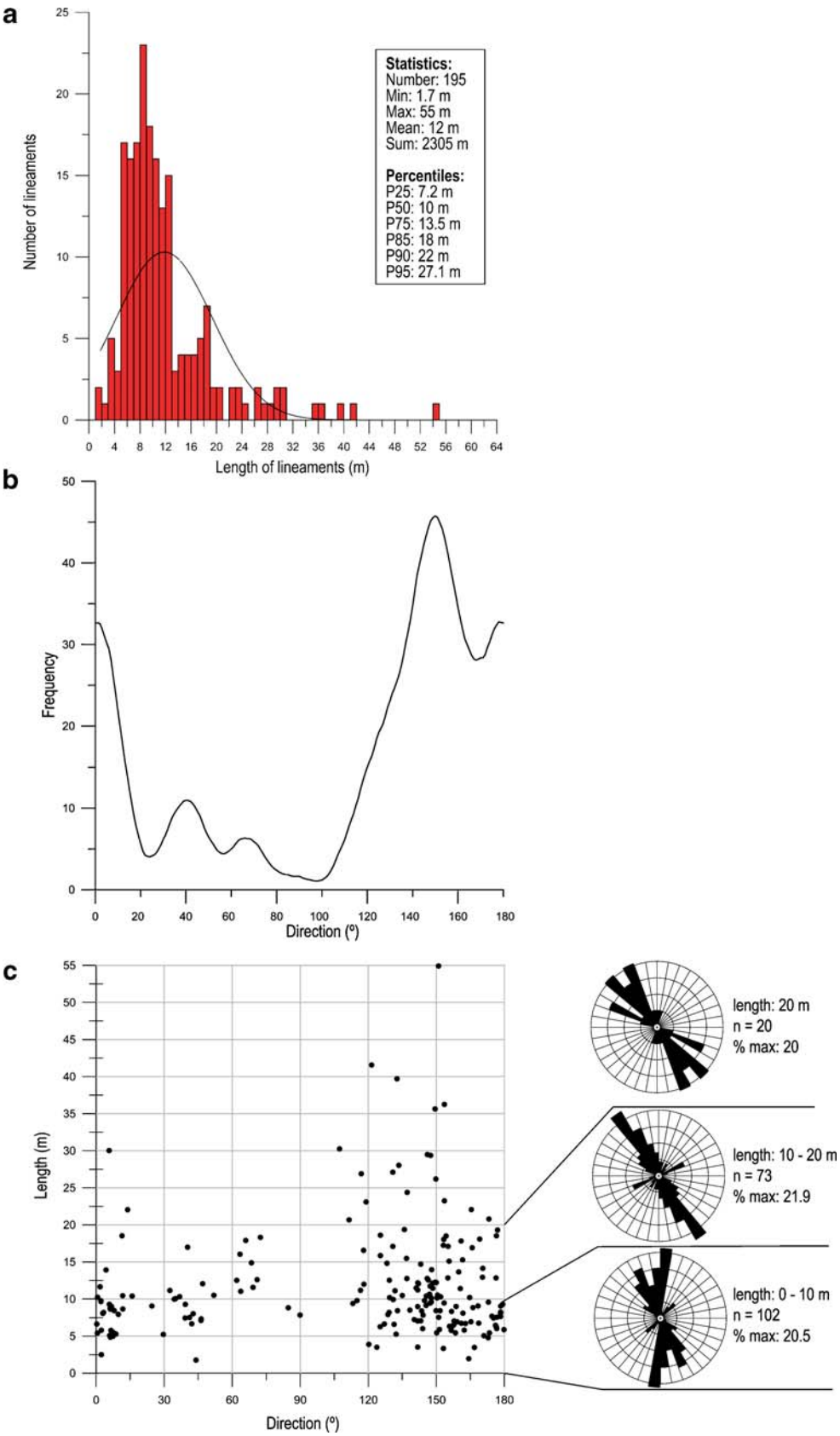


**Fig. 4** **a** Frequency curve of fracture orientation in volcanic rock outcrops of the Alboran Island inner shelf. **b** Relationship between fracture orientation and length. Rose diagrams to the *right* indicate fracture orientation by length intervals. **c** Histogram of the length distribution of fractures

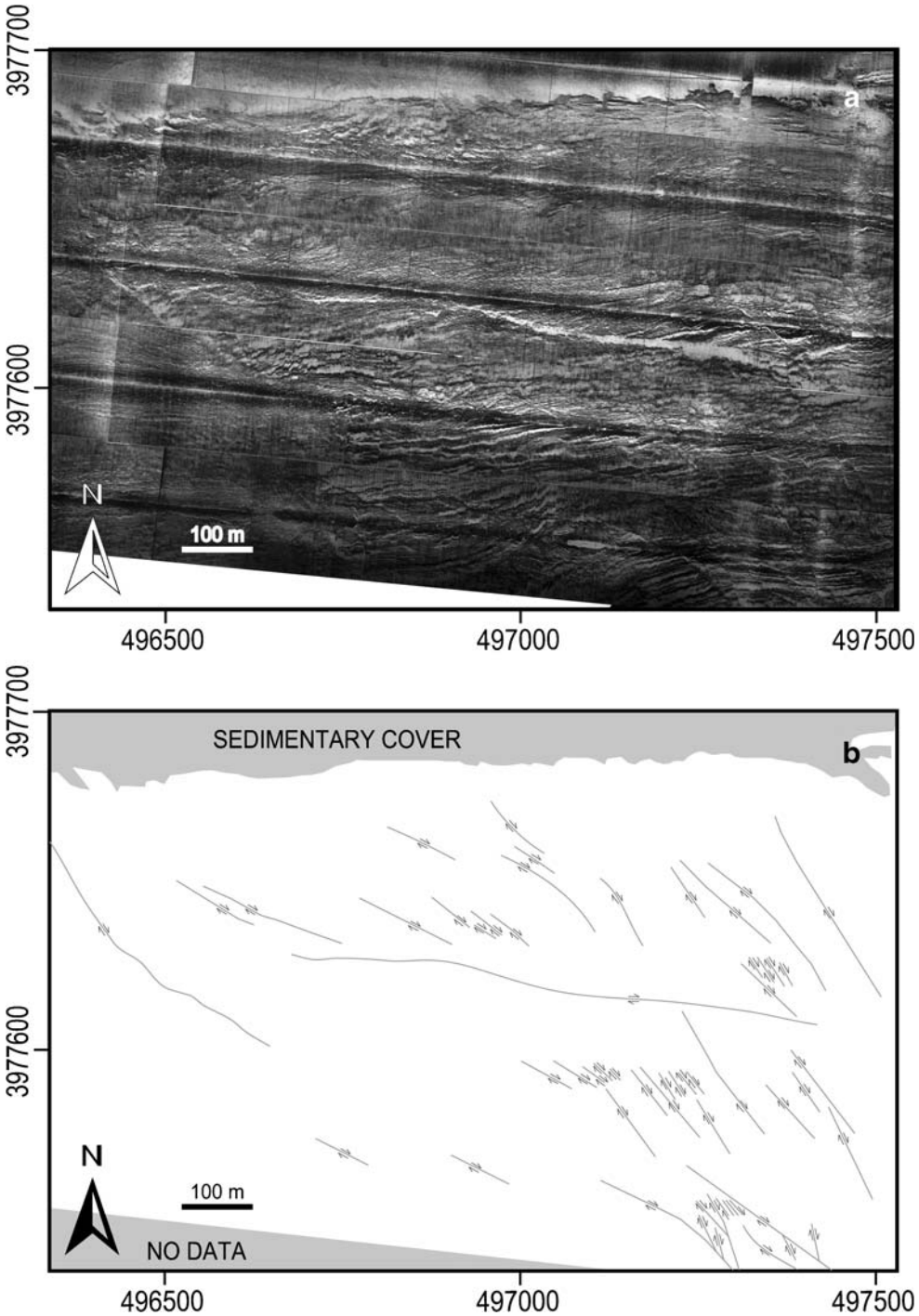


**Fig. 5** **a** Side-scan sonar image from the north-eastern sector of the study area (for location, see Fig. 2). **b** Fracture sketch identified in volcanic outcrop where it is possible to determine the direction of fracture plane movement on the basis of the relative displacement of bed lines

means of an automatic program (Triangle, by J. Bernal, unpublished data) as the arithmetic mean of the three sides of each triangle (Fig. 3b). To display the variations of this distance and the most representative distances from their distribution over the area, a contour map of average distances between fractures was drawn (Fig. 3c).

## Results

From the analysis of the side-scan sonar mosaic, a total of 195 fractures were mapped in the volcanic rock outcrops of the Alboran Island inner shelf (Fig. 2b). The length of fractures varies from 1.7 to 55 m. Their size distribution is

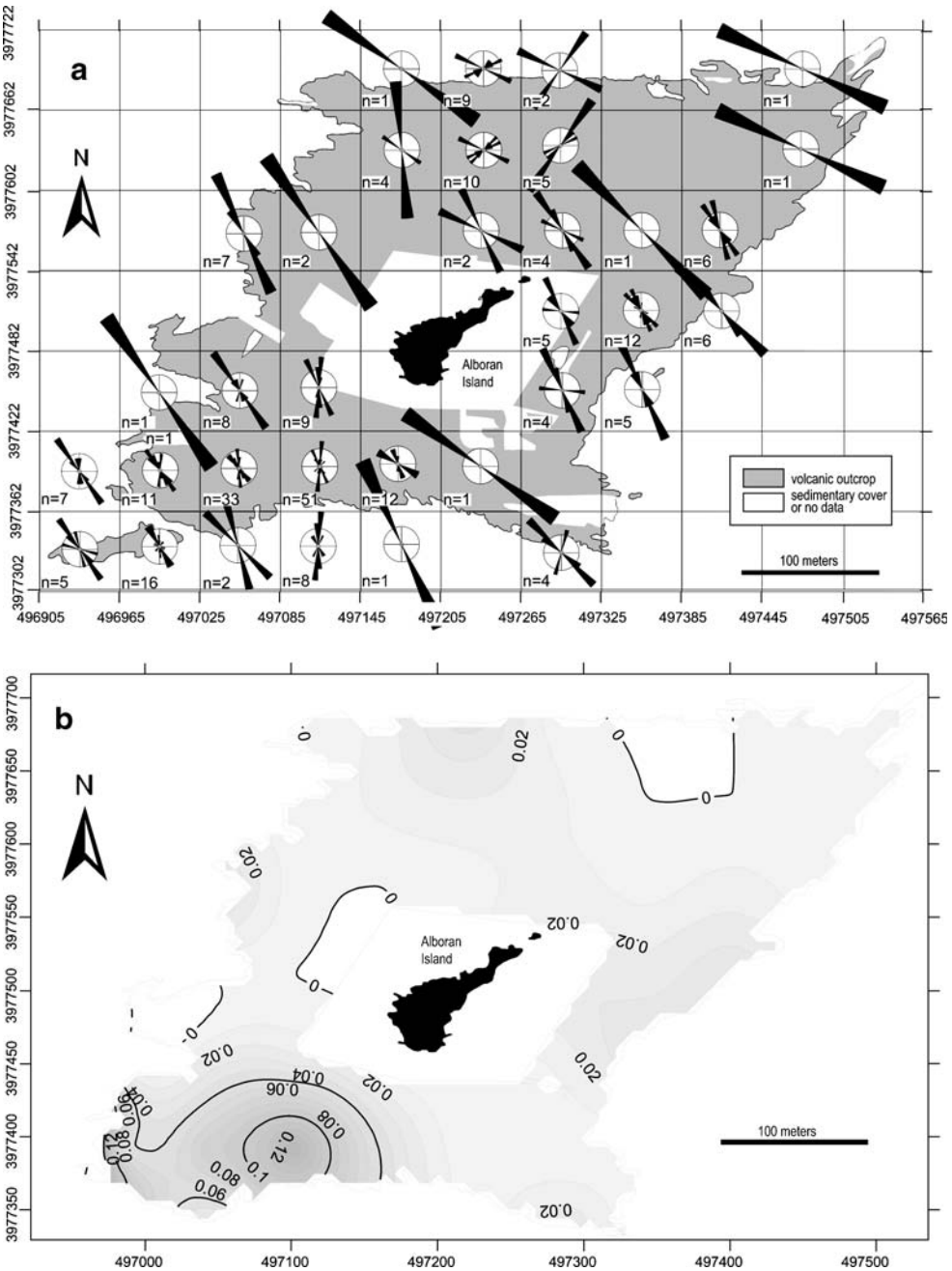


**Fig. 6** **a** Variations in fracture distribution across the study area, in a grid of cells of 60×60 m. *Outer circles* in the rose diagrams represent 20% of data. **b** Contour map of fracture density. Isoline values represent density calculated as length of fracture per square meter using a grid of 60×60 m cells

log-normal, with a mode of 8–9 m (Fig. 4a). The orientations of the fractures in the area are represented by rose diagrams (Fig. 2c). To avoid the influence of line-segmentation number, fracture trace length was weighted in the statistical analysis of fracture direction (Fig. 2d).

## Orientation

Maximum orientation of volcanic rock fractures on the Alboran Island inner shelf is clearly NW–SE, with a dispersion of about 50° (Fig. 4b); other secondary maxima are NNE–SSW, NE–SW and ENE–WSW. Moreover, it is possible to determine the direction of movement of some fracture planes on the basis of the relative displacement of bed lines (Fig. 5); NW–SE to NNW–SSE fractures show right-lateral strike-slip, NNE–SSW fractures left-lateral strike-slip movement.

Relationships between direction and length (Fig. 4c) indicate that NW–SE to NNW–SSE fracture orientations, and fracture lengths from 2 m to longer than 20 m are the most common. NNE–SSW fractures are dominant in the 2–10 m interval; also, NE–SW-trending fractures show a secondary maximum in the same interval. A secondary maximum of ENE–WSW-trending fractures is evident in

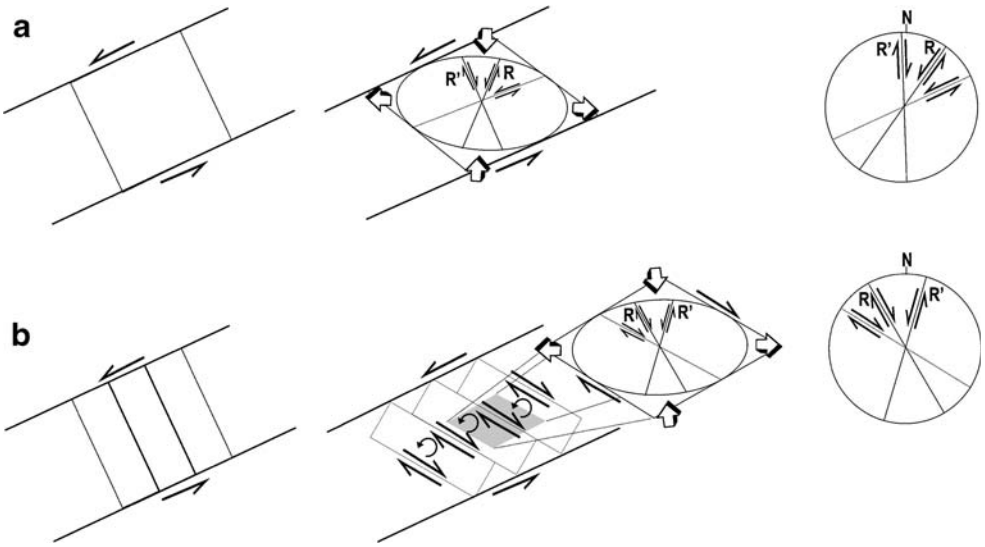


**Fig. 7** **a**, **b** Simplified sketch of fracture patterns in left-lateral wrench situations: **a** simple parallel wrenching, **b** block rotation related to simple parallel wrenching, and new fracture patterns associated with simple parallel wrenching in the block boundary

the 10–20 m interval. Moreover, it was possible to establish a secondary maximum of WNW–ESE fracture direction for fracture lengths longer than 20 m. An important aspect of length–orientation relationships is the decreasing occurrence of NNE and NE–ENE fractures with increasing length.

Spatial variation in fracture orientation was calculated by means of a grid of square cells, representing the length and number of fractures in each cell (Fig. 6a). The results show a ubiquitous pattern of dominant NW–SE direction, with secondary maxima similar to those obtained in the analysis of the total data. Fractures with NW–SE direction are present in the entire study area. Nevertheless, there are other fracture directions which characterize certain locations: (1) fractures with NNW–SSE orientation are situated in the southwest (between horizontal reference lines 3977302 and 3977422, Fig. 6a) and the west (between vertical reference lines 497265 and 497445, Fig. 5a); (2) fractures with WNW–ESE orientation are observed in the north (between horizontal reference lines 3977542 and 3977722, Fig. 6a) and the west (between vertical reference lines 497265 and 497325, Fig. 6a); (3) in some places in the north, a NE–SW direction becomes more evident (between horizontal reference lines 3977602 and 3977722, Fig. 6a).

### Density

The mean average distance between fractures in the continental shelf volcanic outcrops is 30 m (Fig. 3b). The mode of about 7 m is very similar to that of the fracture length (Fig. 4a). The cumulative percentage $\Phi_{85}$ is about 55 m. The contour map of distance between fractures (Fig. 3c) shows that, in most parts of the study area, the distance between lineaments varies between 1 and 60 m.

For a density map to be geologically meaningful, the minimum cell size must be greater than the distance between fractures previously calculated (Cortés et al. 2003). To calculate fracture density, several tests were made with cells of different sizes. Within this context, it should be noted that a contour map drawn from a cell size which is obviously too small (30×30 m) is no better than a simple fracture map, since about 41% of cell values are null. We eventually chose a cell size of 60×60 m (about two times the average spacing of fractures) in order to draw a geologically meaningful outcrop-scale map (Fig. 6b), thereby achieving reasonable accuracy and a minimum of cells with null values between fractures (cf. only 15% of cell values were null).

Several fracture density minima (west and southeast of the island) are the result of poor signal quality of the side-scan sonar images. Fracture density maxima within volcanic outcrops on the inner continental shelf are located (Fig. 6b) on the south-western border and along the northern and eastern edge.

## Discussion

Fracture density variations in the study area can be correlated with underlying macrostructures associated with the pre-Neogene basement (see Fig. 1a). The relationship is made particularly clear by comparing the fracture density maximum with macrostructure orientation. In this area, fracture density is higher in certain zones, with contours elongate and parallel to the dominant NW–SE structures described by several authors in the vicinity (e.g. Woodside and Maldonado 1992; Vázquez et al. 2000; Marín-Lechado et al. 2005). Such a relationship may be the result of large structures acting as inhomogeneities and ‘stress raising

zones' (Pollard and Segall 1987; Sassi et al. 1993; Sassi and Faure 1997).

Although fracture orientation in the volcanic outcrops is variable (see Fig. 2b), the NW–SE absolute maximum of fracture orientation is evident throughout the study area. This directional maximum correlates well with one of the two fault and fold maxima mapped in the basement rock (Fig. 1a). Since these orientations coincide, fracture formation in the Upper Miocene probably relates to basin floor anisotropy. Reactivation of faults in pre-Neogene rocks during the Upper Miocene–Quaternary has been observed in several onshore and offshore areas of the Alboran Sea (among others, by Gensous et al. 1986; De Larouzière et al. 1988; Woodside and Maldonado 1992; Watts et al. 1993). That the basin basement fault pattern should be the same as that of the volcanic outcrops seems a reasonable assumption.

Given the fracture orientation, we propose that these faults are the result of reactivation of similarly oriented basement faults in the Alboran Basin. The basement fault relationship with counterparts in the Upper Miocene volcanic cover cannot, however, be inferred directly. Analogue model studies suggest that basement fault movement produces a set of minor tectonic structures in the cover. Fractures/faults in the cover, not necessarily located directly above the basement fault, may have occurred within an upward-opening fan of minor faults (Horsfield 1977; Naylor et al. 1986; Mandl 1988; Withjack et al. 1990). At the surface, these fractures develop along a band located over the main basement fault. Their orientation depends on (1) the strike-slip/dip–slip relationships of the basement fault, (2) the mechanical and geometrical characteristics of the cover, and (3) the magnitude of the stress-inducing deformation.

The late Tortonian and Messinian stress field direction was shown, from meso-structural analysis, to reflect roughly NNW–SSE to N–S compression (Montenat et al. 1987; Sanz de Galdeano 1990). The left-lateral northeast strike-slip faults were activated at that time. Intense tectonic deformation occurred along the Alboran Ridge, which has reacted by transpression, as would be the case in an enormous positive flower structure (Bourgois et al. 1992). The N–S Recent stress field direction has also favoured left-lateral movement along the northeast-trending faults (Philip 1987). Wrenching produced two main sets of intersected vertical fractures along the wrench zone. One set, the low-angle fractures, has angles between 10 and 30° relative to the wrench strike, and the same displacement direction as that of the main wrench zone and final wrench fault. The other set, i.e. the high-angle fractures, intersects the wrench at angles of between 70 and 90°, and has a displacement direction opposite to that of the wrench. These conjugate fractures can take the form of either joints or faults, or both, depending on the magnitude of wrenching (Wilcox et al. 1973). The low- and high-angle conjugate fractures have been termed Riedel shears (R) and conjugate Riedel shears (R′) respectively by Tchalenko and Ambraseys (1970).

If fractures affecting volcanic rock around the Alboran Island originated from simple shear movement along the ENE–WSW Alboran Ridge edge faults, then Riedel shears would trend NE and N (see Fig. 7a). However, in our case the NE–SW fracture (R) direction of movement is left-lateral, whereas the N–S fracture (R′) direction of movement is right-lateral. This fracture pattern is not coincident with the fracture pattern observed in the volcanic outcrops. Nevertheless, if previous anisotropy were oriented obliquely to the wrench direction, then movement of the main faults would produce external rotational deformation of the individualized crustal blocks (Fig. 7b). Wrenching forces, which result from simple regional shear, act in opposite directions, as if on separate parallel lines, so as to form a couple. The resulting deformation is generally restricted to a linear wrench zone, parallel to the couple and to the edges of the moving crustal blocks. A left-lateral wrench has an external direction of rotation which is counter-clockwise. Edges between blocks act as individualized wrench zones, and tend to deform somewhat independently. Therefore, if shear is concentrated along WNW–ESE faults reactivated by left-lateral strike-slip movement of faults located in Alboran Ridge margins, then orientation of the main conjugate Riedel fractures will trend NW to NNW (R, with right-lateral strike-slip movement) or NNE (R′, with left-lateral strike-slip movement). The foregoing would explain the orientation and direction of fracture movement observed in the volcanic outcrops on the inner continental shelf of Alboran Island.

## Conclusions

Study of side-scan sonar imagery of volcanic outcrops on the inner continental shelf of Alboran Island proved useful in the analysis of recent, visually inspected fracture patterns.

The absolute maximum of fractures, NW–SE with a dispersion of about 50°, is fairly ubiquitous in the study area. Other relative maxima are NNE–SSW, NE–SW and ENE–WSW.

Average distances between fractures, ranging from 1 to 60 m, were calculated by means of triangulation. The best-fitting grid square with which to calculate geologically meaningful density (length of fractures per $km^2$) was found to be 60×60 m.

Density contour maxima elongation in the NW–SE direction, coincident with one main structural orientation,

suggests that fracture density is controlled by large structures underlying volcanic rock outcropping around Alboran Island.

Fracturing in Upper Miocene volcanic rock could result from reactivation of faults trending NE and WNW to NW within the Alboran basin basement. Left-lateral strike-slip displacement of NE–SW-oriented faults along the Alboran Ridge edges caused the counter-clockwise rotation of the various blocks which compartmentalize the ridge. These blocks are bounded by WNW–ESE and NW–SE fractures which were reactivated with right-lateral strike-slip movement. Wrenching caused two main sets of conjugate fractures trending NNW and NNE. NNW–SSE fracture movement is right-lateral strike-slip, associated with Riedel shear fractures (R). NNE–SSW fracture movement has a left-lateral strike-slip component, and can be related to conjugate Riedel shear fractures (R′). As inferred from fault population analysis, reactivation of faults was probably due to a NW–SE-oriented compressional stress field regime active during the late Tortonian and Messinian, or in more recent times.

**Acknowledgements** We thank Burg Flemming, Jesús Galindo-Zaldívar and an anonymous referee for providing corrections and constructive comments which significantly improved the manuscript. The authors are grateful to the Instituto Español de Oceanografía, and the officers and crew of the B/O F.P. Navarro for their assistance at sea, and to Dr. Javier Bernal (CAMD-NIST, USA) who developed the TRIANGLE program for application of the Delaunay method. This is a contribution to the project CONSOLIDER-INGENIO 2010 CSD2006-0041-TOPOIBERIA.

## References

Bárcenas P, Vázquez JT, Díaz del Río V, Fernández-Salas LM, Tello O, Sanz JL (2000) La vertiente meridional del Banco de la isla de Alborán: presencia de dos sistemas cañón-abanico submarino. In: Ext Abstr Vol VI Reunión Nacional de Geomorfología, 17–20 September 2000, Madrid University, pp 169

Bourgois J, Mauffret A, Ammar A, Demnati A (1992) Multichannel seismic data imaging of inversion tectonics of the Alboran Ridge (Western Mediterranean Sea). Geo Mar Lett 12:117–122

Campos J, Maldonado A, Campillo AC (1992) Post-messinian evolutional patterns of the central Alboran Sea. Geo Mar Lett 12:173–178

Casas AM, Cortés AL, Maestro A, Soriano MA, Riaguas A, Bernal J (2000) LINDENS: a basic program for lineament analysis. Comput Geosci 26:1011–1022

Comas MC, García-Dueñas V, Jurado MJ (1992) Neogene tectonic evolution of the Alboran Sea from MCS data. Geo Mar Lett 12:157–164

Cortés AL, Soriano MA, Maestro A, Casas AM (2003) The role of tectonic inheritance in the development of recent fracture systems, Duero Basin, Spain. Int J Remote Sens 24:4325–4345

De Graciansky PC, Dardeau G, Lemoine M, Tricart P (1989) The inverted margin of the French Alps and foreland basin inversion. In: Cooper MA, Williams GD (eds) Inversion tectonics. Geol Soc Special Pub 44:87–104

De Larouzière FD, Bolze J, Bordet P, Hernández J, Montenat C, Ott d'Estevou P (1988) The Betic segment of the lithospheric trans-Alboran shear zone during the Late Miocene. Tectonophysics 152:41–52

De Mets C, Gordon RG, Argus D, Stein S (1990) Current plate motions. Geophys J Int 101:425–478

Dewey JF, Helman ML, Turco E, Hutton DHW, Knott SD (1989) Kinematics of the western Mediterranean. Geol Soc Lond Special Pub 45:265–283

Dillon WP, Robb SM, Gary Greene M, Lucena JC (1980) Evolution of the continental margin of southern Spain and the Alboran Sea. Mar Geol 36:205–226

Duggen S, Hoernle K, Bogaard P, Harris C (2004) Magmatic evolution of the Alboran region: the role of subduction in forming the western Mediterranean and causing the Messinian Salinity Crisis. Earth Planet Sci Lett 218:91–108

Gensous B, Tesson MR, Winnock E (1986) La marge méridionale de la Mer d'Alboran: caractères structuro-sédimentaires et évolution récente. Mar Geol 72:341–370

Hernández-Pacheco A, Ibarrola E (1970) Nuevos datos sobre la petrología y geoquímica de las rocas volcánicas de la Isla de Alborán (mediterráneo Occidental, Almería). Estud Geol 26:93–103

Horsfield WT (1977) An experimental approach to basement-controlled faulting. Geol Mijnb 56:363–370

Leblanc D (1990) Tectonic adaptation of the external zones around the curved core of an orogen: the Gibraltar Arc. J Struct Geol 12:1013–1018

Maldonado A, Campillo AC, Mauffret A, Alonso B, Woodside JM, Campos J (1992) Alboran Sea Late Cenozoic tectonic and stratigraphic evolution. Geo Mar Lett 12:179–186

Mandl G (1988) Mechanics of tectonic faulting. Models and basic concepts. Developments in Structural Geology 1. Elsevier, Amsterdam

Marín-Lechado C, Galindo-Zaldívar J, Rodríguez-Fernández LR, Pedrera A (2005) Active faults, seismicity and stresses in an internal boundary of a tectonic arc (Campo de Dalías and Níjar, southeastern Betic Cordilleras, Spain). Tectonophysics 396:81–96

Mauffret A, El-Robrini M, Gennesseaux M (1987) Indice de la compression récent en mer Méditerranée: un bassin losangique sur la marge nord-algérienne. Bull Soc Geol Fr 8:1195–1206

Mauffret A, Maldonado A, Campillo AC (1992) Tectonic framework of the eastern Alboran and western Algerian basins, western Mediterranean. Geo Mar Lett 12:104–110

Montenat C, Ott d'Estevou P, Masse P (1987) Tectonic and sedimentary characters of the Betic Neogene basins evolving in a crustal transcurrent shear zone (southeast Spain). Bull Centre Rech Explor-Prod Elf-Aquitaine 11:1–22

Naylor MA, Mandl G, Sijpesteijn CHK (1986) Fault geometries in basement-induced wrench faulting under different initial stress states. J Struct Geol 8:737–752

Ott d'Estevou P, Montenat C (1985) Evolution structurale de la zone bétique orientale (Espagne) du Tortonien à l'Holocène. C R Acad Sci Paris 300:363–368

Philip H (1987) Plio-Quaternary evolution of the stress field in the Mediterranean zones of subduction and collision. Ann Geophys 5B:301–320

Pollard DD, Segall P (1987) Theoretical displacements and stresses near fractures in rock, with application of faults, joints, veins, dikes, and solution surfaces. In: Atkinson BK (ed) Fracture mechanics of rocks. Academic, London, pp 277–349

Preparata FP, Shamos MI (1985) Computational geometry—an introduction. Springer, Berlin

Rehault JP, Boillot G, Mauffret A (1985) The western Mediterranean Basin. In: Stanley DJ, Wezel FC (eds) Geological evolution of the Mediterranean Basin. Springer, Berlin, pp 101–130

Riedel W (1929) Zur Mechanik geologischer Brucherscheinungen. Zentralb Mineral Geol Paläontol B:354–368

Roest WR, Srivastava SP (1991) Kinematics of the plate boundaries between Eurasia, Iberia, and Africa in the north Atlantic from the Late Cretaceous to present. Geology 19:613–616

Sanz de Galdeano C (1990) Geologic evolution of the Betic Cordilleras in the western Mediterranean, Miocene to the present. Tectonophysics 172:107–119

Sassi W, Faure JL (1997) Role of faults and layer interfaces on the spatial variation of stress regimes in basins: inferences from numerical modelling. Tectonophysics 266:101–119

Sassi W, Colletta B, Balé P, Paquereau T (1993) Modelling of structural complexity in sedimentary basins: the role of pre-existing faults in thrust tectonics. Tectonophysics 226:97–112

Srivastava SP, Roest WR, Kovacs LC, Oakey G, Lévesque S, Verhoef J, Macnab R (1990) Motion of Iberia since Late Jurassic: results from detailed aeromagnetic measurements in the Newfoundland Basin. In: Boillot G, Fontboté JM (eds) Alpine evolution of Iberia and its continental margins. Tectonophysics 184:229–260

Tchalenko JS (1970) Similarities between shear zones of different magnitudes. Geol Soc Am Bull 81:1265–1640

Tchalenko JS, Ambraseys NN (1970) Structural analysis of the Dasht-e Baÿaz (Iran) earthquake fractures. Geol Soc Am Bull 81:41–60

Vázquez JT, Bárcenas-Gascón P, Díaz-del-Río V, Sanz JL (2000) Características morfoestructurales del entorno sumergido de la Isla de Alborán. Geotemas 1(4):235–238

Watts AB, Platt JP, Buhl P (1993) Tectonic evolution of the Alboran Sea Basin. Basin Res 5:153–177

Wilcox RE, Harding TP, Seely DR (1973) Basic wrench tectonics. AAPG Bull 57:74–96

Williams GD, Powell CM, Cooper MA (1989) Geometry and kinematics of inversion tectonics. In: Cooper MA, Williams GD (eds) Inversion tectonics. Geol Soc Special Pub 44:3–15

Withjack MO, Olson J, Peterson E (1990) Experimental models of extensional forced folds. AAPG Bull 74:1038–1054

Woodside JM, Maldonado A (1992) Styles of compressional neo-tectonics in the Eastern Alboran Sea. Geo Mar Lett 12:111–116